Functional Mapping of Flow and Back-Diffusion Rate of N-Isopropyl-*p*-Iodoamphetamine in Human Brain

Yoshiharu Yonekura, Sadahiko Nishizawa, Takao Mukai, Yasushi Iwasaki, Hidenao Fukuyama, Masatsune Ishikawa, Nagara Tamaki and Junji Konishi

Kyoto University Faculty of Medicine and Kyoto College of Medical Technology, Kyoto, Japan

Iodine-123-labeled N-isopropyl-*p*-iodoamphetamine (IMP) has been reported to be an excellent tracer for mapping cerebral blood flow with single-photon emission computed tomography (SPECT). Clinical interpretation of these SPECT images, however, requires further understanding of the kinetics of IMP in the human brain. In order to evaluate the kinetic behavior of IMP in normal and diseased areas, we measured flow and back-diffusion rates with serial dynamic SPECT scans following an intravenous bolus injection of IMP using a multi-detector SPECT scanner. Arterial input function was determined by octanol extracted radioactivity of serial arterial blood samples. Average values for influx rate (K_1) and back-diffusion rate (k_2) were 0.43 ml/g/min and 0.014 min^{-1} in the normal cerebral cortex, 0.43 and 0.013 in the basal ganglia, 0.28 and 0.012 in the white matter and 0.48 and 0.016 in the cerebellar hemisphere. The partition coefficient (K_1/k_2 ratio) was 32.4 ml/g in the cerebral cortex, 35.3 in the basal ganglia, 24.7 in the white matter and 30.4 in the cerebellum. The K_1-to-k_2 ratio in the infarcted and ischemic regions as well as in the tumor was smaller than that of the normal cortex. Accurate measurement of local cerebral blood flow (LCBF) based on the microsphere model was possible only on the early SPECT images, but a relative pattern of LCBF can be assessed with SPECT images obtained within 1 hr after injection except for tumors.

J Nucl Med 1993; 34:839–844

Iodine-123-labeled N-isopropyl-*p*-iodoamphetamine (IMP) has been used to map brain perfusion with single-photon emission computed tomography (SPECT) (*1,2*). By taking advantage of the high extraction and the subsequent retention of this tracer in the brain (*3*), Kuhl et al. proposed to use IMP for measurement of local cerebral blood flow (LCBF) with SPECT, based on the microsphere model (*2*). Because of its excellent first-pass extraction, the initial distribution of this compound was reported to be linearly correlated with blood flow (*2,4*). Recent studies with dynamic SPECT, however, suggested regional differences of IMP kinetics in the human brain both in the normal brain structures and between normal and diseased regions (*4–8*).

Ideally, to obtain accurate regional cerebral blood flow information with IMP, one should acquire SPECT data as early as possible after injection, yet most SPECT studies are performed over 30 min after injection using a rotating gamma camera system. Therefore, it is important to evaluate the significance of IMP kinetics to understand both tracer behavior as well as clinical interpretation of SPECT images. In order to examine the regional kinetics of IMP in the human brain, we performed serial dynamic SPECT imaging using a multi-detector SPECT scanner (*9*) with arterial blood sampling and measured the influx and back-diffusion rates of IMP in normal and diseased regions based on a two-compartment model.

MATERIALS AND METHODS

Subjects

Six patients (five males and one female) were studied (Table 1). Four patients had cerebrovascular disease, including two with cerebral infarction, one with occlusion of the right internal carotid artery without major infarction and one with arteriovenous malformation. The other two subjects included one patient with oligodendroglioma and one normal subject originally suspected of having cerebrovascular disease but diagnosed as normal by x-ray computed tomography and contrast angiography.

Radiopharmaceuticals

We used commercially supplied IMP (0.45 mg of N-isopropyl-*p*-iodoamphetamine hydrochloride in 3 ml saline solution) labeled with 3 mCi of ^{123}I (Nihon Medi-Physics, Nishinomiya, Japan). The subject received a bolus injection of IMP via a cubital vein. To block the accumulation of free radioactive iodine by the thyroid, potassium iodide (30 mg/day) was given for 4 days starting the day before the study.

Data Acquisition

A dynamic SPECT scan was obtained with a multi-detector ring-type SPECT scanner (Shimadzu Co., Kyoto, Japan). The scanner consisted of three detector rings at 30-mm intervals with

Received Aug. 13, 1992; revision accepted Jan. 18, 1993.

For correspondence or reprints contact: Yoshiharu Yonekura, MD, Dept. of Brain Pathophysiology, Kyoto University Faculty of Medicine, 54 Shogoin Kawahara-cho, Sakyo-ku, Kyoto 606-01, Japan.

TABLE 1
Clinical Diagnosis of Patients Studied

Patient	Age	Sex	Clinical diagnosis
H.K.	68	F	Cerebral infarction
H.K.	45	M	Occlusion of right internal carotid artery
A.M.	65	M	Cerebral infarction
M.U.	56	M	Normal
K.H.	32	M	Arteriovenous malformation
Y.N.	18	M	Oligodendroglioma

128 sodium iodide crystals in each ring. The use of a special long turbofan collimator designed for brain SPECT imaging provided a spatial resolution of 11 mm FWHM at the center of the transaxial plane with a sensitivity of 6.6 kcps/μCi/ml/slice. The axial resolution was 23.5 mm FWHM (*9*).

The subject's head was positioned in the gantry parallel to the orbitomeatal (OM) line, and the center of the bottom slice was aligned to 2 cm above the OM line so that a total of three slices corresponding to 2, 5 and 8 cm above the OM line were obtained. A serial SPECT scan was performed every 2.5 min for 60 min postinjection. All SPECT images were reconstructed using a filtered back-projection algorithm with a Shepp-Logan filter convoluted with a Butterworth filter (cut-off frequency 0.3 and order 4) (*10*). Attenuation correction was performed using the corrected geometric mean approach (*11*), assuming that the head is an ellipsoid shape with a uniform attenuation coefficient of 0.05/cm.

Serial arterial blood samples were taken during the SPECT scan through a small catheter inserted in the radial artery. The sampling interval was 15 sec during the initial 1 min and less frequent in the later periods. These blood samples were extracted by octanol to obtain lipophilic activity in the blood. Cross-calibration of the SPECT images and the radioactivity in the arterial blood samples (measured by the well counter) was performed by scanning a 20-cm diameter cylindrical phantom containing six "pie"-shaped compartments filled with different concentrations of ^{123}I solution (*12*).

Kinetic Analysis

We assumed a simple two-compartment model as shown in Figure 1. In this kinetic model, IMP is delivered by blood flow and extracted in the brain but is gradually washed out from the tissue. The blood compartment represents lipophilic tracer in arterial blood at concentration $C_a(t)$, while $C_b(t)$ denotes tracer concentration in brain tissue. From this model, the following differential equation is given:

$$dC_b(t)/dt = K_1 \cdot C_a(t) - k_2 \cdot C_b(t). \quad \text{Eq. 1}$$

In solving this equation, we have

$$C_b(t) = K_1 \cdot \exp(-k_2 \cdot t) * C_a(t), \quad \text{Eq. 2}$$

where * denotes the operation of convolution. The rate constant K_1 is described as

$$K_1 = F \cdot E, \quad \text{Eq. 3}$$

where F is the flow rate of blood per unit mass of the brain tissue and E is the single-pass extraction ratio of IMP in the brain. The ratio of K_1 and k_2 corresponds to the partition coefficient of the tracer. Based on this kinetic model, K_1 and k_2 were estimated in each pixel of the SPECT images to create functional mapping of these parameters by the least-squares curve fitting procedure by applying the Newton-Raphson method (*13,14*).

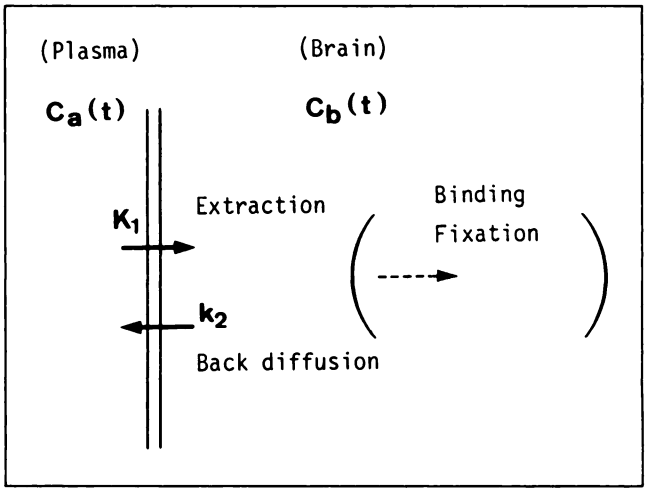

FIGURE 1. Two-compartment model of IMP.

Calculation of LCBF using the simple arterial sampling method without consideration of back-diffusion (microsphere model) was also applied for quantitative measurement of LCBF with IMP SPECT images. The assumption of complete extraction of tracer in the brain (E = 1) and no back-diffusion (k_2 = 0) in the above equation provides:

$$C_b(t) = F \int_0^T C_a(t)\, dt \quad \text{Eq. 4}$$

$$F = C_b(t) \Big/ \int_0^T C_a(t)\, dt. \quad \text{Eq. 5}$$

According to Equation 5, the SPECT images obtained at 5, 30 and 60 min after injection were converted to the LCBF map with the same input function used in the previous calculation.

Regions of interest (ROIs) were placed manually with a light pen over the frontal, parietal, temporal and occipital cortex, basal ganglia, white matter region and cerebellum in both hemispheres. The normal subject and the nondiseased hemisphere in the patients with unilateral disease were selected to calculate the parameters in normal brain structures. To obtain values in the diseased area, similar size ROIs were placed over the infarcted area and tumor according to x-ray computed tomography (CT) results, and the ischemic area was selected as the area showing decreased IMP uptake in the early SPECT images with normal x-ray CT images.

Statistical analysis was performed by paired or unpaired Student's t-test, and p values less than 0.05 were considered significant.

RESULTS

Table 2 and Figure 2 show the summary of parameters. In normal brain structures, K_1 was highest in the cerebellum, but all other gray matter regions showed similar values. On the other hand, larger k_2 values were observed both in the cerebellum and in the occipital cortex, reflect-

TABLE 2
K_1, k_2 and K_1/k_2 in Normal and Diseased Regions*

	K_1 (ml/min/g)	k_2 (min^{-1})	K_1/k_2 (ml/g)
Normal structures			
Cerebellum	0.476 (0.038)	0.0164 (0.0045)	30.4 (5.9)*
Cortex (F,T,P)	0.431 (0.077)	0.0138 (0.0037)	32.4 (6.6)*†‡
Cortex (O)	0.443 (0.074)	0.0165 (0.0042)	27.9 (5.1)*†‡
Basal ganglia	0.433 (0.076)	0.0128 (0.0037)	35.3 (6.6)*†‡
White matter	0.279 (0.059)	0.0119 (0.0032)	24.7 (6.8)*†‡
Diseased regions			
Infarction	0.128 (0.070)	0.0110 (0.0053)	11.3 (2.0)‡§
Ischemia	0.209 (0.055)	0.0108 (0.0034)	19.8 (2.2)‡§
Tumor	0.845	0.0810	10.4

*$p < 0.05$, †$p < 0.01$, ‡$p < 0.001$.
§Values in the diseased regions were compared with those of the normal cortex (F,T,P).
Mean values with standard deviation (in parentheses) are shown.
F = frontal, T = temporal, P = parietal, O = occipital.

ing faster washout in these regions. The K_1-to-k_2 ratio was highest in the basal ganglia, followed by the cerebral cortex, which includes the frontal, parietal and temporal regions, cerebellum, occipital cortex, and was lowest in the white matter area.

In the diseased regions, these parameters were quite different from the normal values. The K_1 value varied according to the characteristics of the disease. It was decreased in the infarcted and ischemic areas and highest in the tumor. Although k_2 values were generally proportional to K_1 values, the diseased lesion, including ischemia, infarction and tumor, showed smaller K_1-to-k_2 ratios than normal brain structures. The statistical significance of these differences is shown in Table 2. Figure 3 shows an example of functional images in a patient with cerebral infarction of the right occipital lobe. The K_1 image was similar to the early SPECT image obtained from 5 to 20 min after injection.

In order to examine the effect of back-diffusion on the IMP SPECT images, K_1 and LCBF calculated by the microsphere model were compared in each region of the brain as shown in Figure 4. The calculated LCBF values using 5-min SPECT data were almost identical to the K_1 values. However, the latter SPECT data apparently underestimated the calculated flow values, although the correlation between two measurements was still preserved. Figure 5 shows the percentage ratio of calculated LCBF values to the K_1 values. The underestimation was for flow in the tumor and not for rCBF in the patient with tumor.

DISCUSSION

Since the introduction of IMP for SPECT brain perfusion imaging in the early 1980s, it has been widely accepted as a valuable clinical tool. Although IMP has been reported to be an excellent tracer for mapping of cerebral blood flow with SPECT, temporal changes in regional distribution within the brain raise questions regarding the time of SPECT acquisition for accurate evaluation of cerebral blood flow (*4,5,15*). Ideally, one should acquire the SPECT data as early as possible because tracer washout may change the distribution pattern in the later period. However, the rotating gamma camera system, popular in most institutions, requires considerable time for SPECT data acquisition. In addition, gradual washout of IMP from the lungs results in prolonged arterial input to the brain (*6*). Therefore, SPECT data acquisition is often performed more than 30 min after injection.

In a previous study, we discussed regional differences in IMP kinetics among normal brain structures as well as between normal and diseased regions (*5*). The cerebellum and the occipital cortex showed faster washout than other brain structures. In areas with mild hypoperfusion, a relative increase in activity was observed during serial SPECT images acquired over several hours, resulting in decreased contrast in these regions in late SPECT images. On the other hand, high flow tumors showed rapid washout of IMP. A similar observation was reported in another study (*4*). The present study confirmed these results, indicating that IMP kinetics cannot be explained by the simple flow tracer model.

The retention mechanism of IMP in brain tissue is not clearly understood. Previous studies have reported various explanations for retention, including conversion of lipophilic IMP to the hydrophilic metabolites, pH gradient between blood and brain and affinity with high-capacity and relatively nonspecific binding sites. The variation in partition coefficients among brain structures might be due to different affinities at various binding sites, differences in tissue pH or metabolism or changes in membrane permeability.

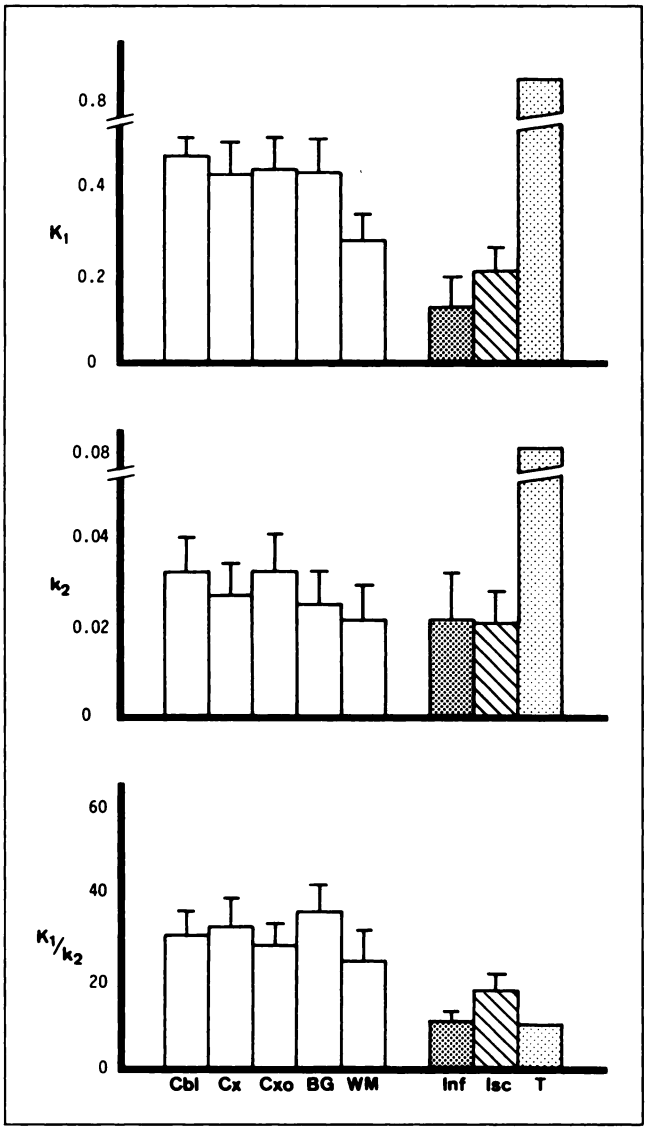

FIGURE 2. K_1, k_2 and K_1/k_2 (mean ± s.d.) in normal brain structures and diseased regions. Cbl = cerebellum; Cx = frontal, temporal and parietal cortex; Cxo = occipital cortex; BG = basal ganglia; WM = white matter; Inf = infarction; Isc = ischemia; T = tumor.

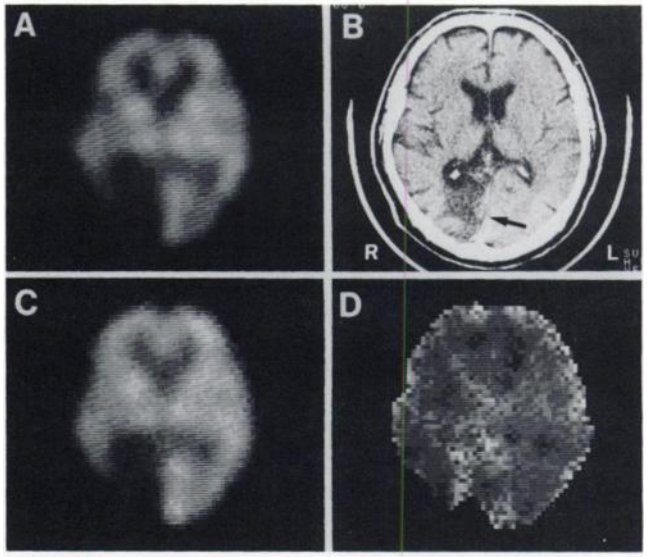

FIGURE 3. Example of functional mapping of IMP in a patient (A.M.) with cerebral infarction. (A) IMP uptake image obtained from 5 to 20 min after injection. (B) X-ray CT image showing low density area in the right occipital region (arrow). (C) Image of K_1 mapping. (D) Image of k_2 mapping.

Decreased K_1/k_2 values of IMP in diseased regions suggest that the mechanism by which IMP is retained in the tissue might reflect some kind of cellular function relating to binding sites, amine metabolism or membrane permeability. This could explain the so-called "redistribution" phenomenon in late SPECT IMP images (*15*). However, the relative distribution of IMP was well preserved during the initial 60 min after injection due to a large partition coefficient, although absolute LCBF values calculated by the microsphere method was significantly underestimated even at 30 min after injection.

Except for high flow tumors, slightly decreased partition coefficients of IMP in diseased regions do not interfere with the clinical value of IMP but may enhance the defect pattern in SPECT images. Moreover, continuous arterial input of IMP from a large lung reservoir cancels intrinsic washout from the brain, which shows a fairly constant activity level for 20–60 min after injection (*16*). Therefore, IMP SPECT images obtained by a rotating gamma camera within 60 min provide sufficient information regarding relative LCBF distribution, although these factors should be carefully considered in the analysis of early and delayed SPECT IMP images.

The present analysis was based on a simple two-compartment model. Heterogeneity of partition coefficients observed in this study, however, suggests that a more complicated model, such as the three-compartment model introducing the third rate constant (k_3) for binding or metabolism, may be suitable for kinetic analysis. In addition to the choice of the kinetic model, this analysis has two major limitations with regards to accurate measurement: (1) absolute quantification of radioactivity was difficult because of the fairly large fraction of undesired scatter radiation and (2) the significant partial volume effect due to low spatial resolution. In spite of these limitations, our data support the validity of brain perfusion SPECT images with IMP. Relative cerebral blood flow pattern (except for tumors) can be evaluated by SPECT images obtained over 30 min after injection, although absolute blood flow quantification should be based on the SPECT images in the initial period.

In conclusion, the present data illustrate regional differences in retention of IMP in normal brain structures and in diseased regions. Accurate measurement of regional cerebral blood flow based on the microsphere model is possible only with early SPECT images obtained

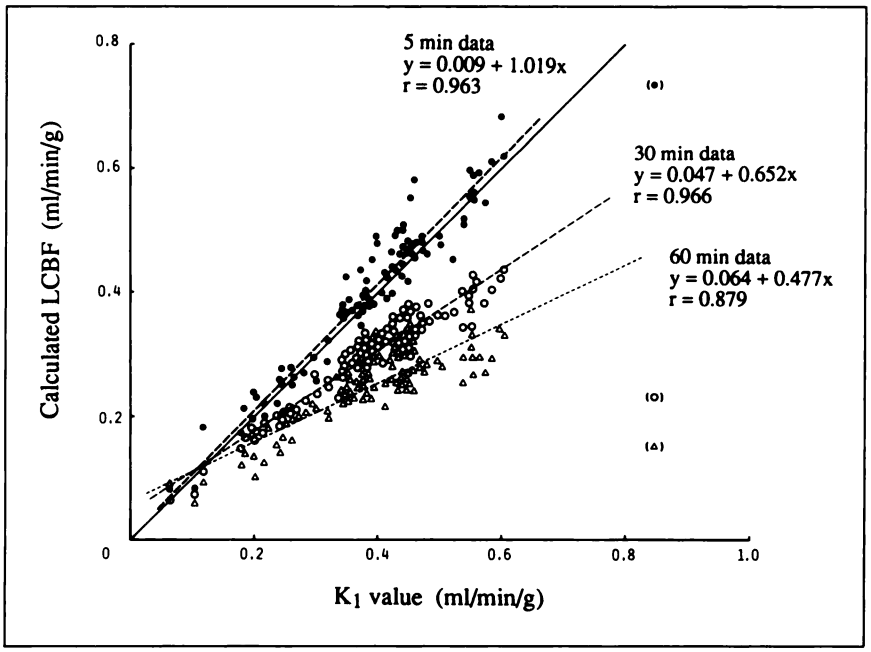

FIGURE 4. LCBF calculated by the microsphere method using SPECT data obtained at 5 min (solid circles), 30 min (open circles) or 60 min (open triangles) in comparison with K_1 values. The regression line (broken line) was almost identical to the line of identity (solid line) for 5-min data. Although the slope decreased with time, the relationship was still linear for 30-min and 60-min data. The tumor, shown in parentheses, was not included for correlation analysis.

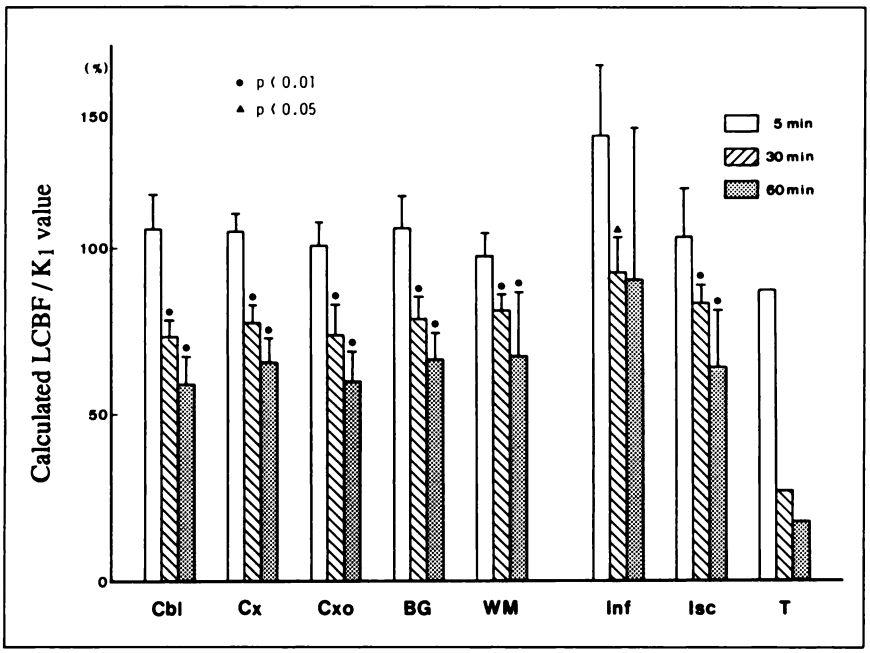

FIGURE 5. Percentage ratio of LCBF calculated by the microsphere method to K_1 values in various regions (mean ± s.d.). Statistical differences to LCBF values obtained with 5-min SPECT data are shown. Abbreviations are same as Figure 2.

shortly after injection. However, the relative pattern of blood flow (except for the tumor) can be measured if the SPECT image was taken within 1 hr. Further studies are needed to clarify the retention mechanism of IMP in normal and diseased areas.

ACKNOWLEDGMENTS

This work was presented at the 38th annual meeting of the Society of Nuclear Medicine, Cincinnati, OH, 1991 and was supported in part by the Japanese Ministry of Education grant 03454282.

REFERENCES

1. Hill TC, Hollman BL, Lovett R, et al. Initial experience with SPECT (single-photon computerized tomography) of the brain using N-isopropyl I-123-*p*-iodoamphetamine: concise communication. *J Nucl Med* 1982;23: 191–195.
2. Kuhl DE, Bario JR, Huang SC, et al. Quantifying local cerebral blood flow by N-isopropyl-*p*-[^{123}I]iodoamphetamine (IMP) tomography. *J Nucl Med* 1982;23:196–203.
3. Winchell HS, Horst WD, Braun L, Oldendorf WH, Hattner R, Parker H. N-isopropyl-[^{123}I]*p*-iodoamphetamine: single-pass brain uptake and washout; binding to brain synaptosomes; and localization in dog and monkey brain. *J Nucl Med* 1980;21:947–952.
4. Nishizawa S, Tanada S, Yonekura Y, et al. Regional dynamics of N-isopropyl-(^{123}I)*p*-iodoamphetamine in human brain. *J Nucl Med* 1989;30: 150–156.

5. Creutzig H, Schober O, Gielow P, et al. Cerebral dynamics of N-isopropyl-(^{123}I)*p*-iodoamphetamine. *J Nucl Med* 1986;27:178–183.
6. Som P, Oster ZH, Yamamoto K, et al. Some factors affecting the cerebral and extracerebral accumulation of N-isopropyl-*p*-iodoamphetamine (IMP). *Int J Nucl Med Biol* 1985;12:185–196.
7. Obrenovitch TP, Clayton CB, Strong AJ. A double-radionuclide autoradiographic method using N-isopropyl-iodoamphetamine for sequential measurements of local cerebral blood flow. *J Cereb Blood Flow Metab* 1987;7:356–365.
8. Baldwin RM, Wu J-L. In vivo chemistry of iofetamine HCL iodine-123 (IMP). *J Nucl Med* 1988;29:122–124.
9. Yonekura Y, Fujita T, Nishizawa S, et al. Multidetector SPECT scanner for brain and body: system performance and applications. *J Comput Assist Tomogr* 1989;13:732–740.
10. Budinger TF, Gullberg GT, Huesman RH. Emission computed tomography. In: Herman GT, ed. *Image reconstruction from projections*. Berlin: Springer-Verlag; 1979:147–246.
11. Sorenson JA. Quantitative measurement of radioactivity in vivo by whole-body counting. In: Hine GJ, Sorenson JA, eds. *Instrumentation in nuclear medicine*. San Diego: Academic Press; 1974:311–348.
12. Eichling JO, Higgins CS, Ter-Pogossian MM. Determination of radionuclide concentrations with positron CT scanning (PETT). *J Nucl Med* 1977;18:845–847.
13. Marquardt DW. An algorithm for least-squares estimation of nonlinear parameters. *J Soc Int Appl Math* 1963;11:431–441.
14. Dell RB, Sciacca R, Lieberman K, Case DB, Cannon PJ. A weighted least-squares technique for the analysis of kinetic data and its application to the study of renal ^{133}Xe washout in dogs and man. *Circ Res* 1973;32:71–84.
15. Raynaud C, Rancurel G, Samson Y. Pathophysiologic study of chronic infarcts with I-123 isopropyl iodo-amphetamine (IMP): the importance of periinfarcted area. *Stroke* 1987;18:21–29.
16. Yonekura Y, Fujita T, Nishizawa S, Iwasaki Y, Mukai T, Konishi J. Temporal changes in accumulation of N-isopropyl-*p*-iodoamphetamine in human brain: relation to lung clearance. *J Nucl Med* 1989;30:1977–1981.

(continued from page 817)

SELF-STUDY TEST
Skeletal Nuclear Medicine

ANSWERS *(continued)*

usually return to normal 12-18 months after injury.

References

1. Desai A, Alavi A, Dalinka M, Brighton C, Esterhai J. Role of bone scintigraphy in the evaluation and treatment of nonunited fractures [Concise Communication]. *J Nucl Med* 1980;21:931-934.
2. Esterhai J, Alavi A, Mandell GA, Brown J. Sequential technetium-99m/gallium-67 scintigraphic evaluation of subclinical osteomyelitis complicating fracture nonunion. *J Orthop Res* 1985;3:219-225.
3. Esterhai JL Jr, Goll SR, McCarthy KE, et al. Indium-111 leukocyte scintigraphic detection of subclinical osteomyelitis complicating delayed and nonunion of long bone fractures: a prospective study. *J Orthop Res* 1987;5:1-6.
4. Hadjipavolu A, Lisbona R, Rosenthall L. Difficulty of diagnosing infected hypertrophic pseudoarthrosis by radionuclide imaging. *Clin Nucl Med* 1983;8:45-49.
5. Matin P. Appearance of bone scans following fractures, including immediate and long-term studies. *J Nucl Med* 1979;20:1227-1231.
6. Rupani HD, Holder LE, Espinola DA, Engin SI. Three-phase radionuclide bone imaging in sports medicine. *Radiology* 1985;156:187-196.

Items 9-13: Three-phase Bone Scintigraphy

Answers: 9, T; 10, F; 11, F; 12, F; 13, F

Focally increased perfusion and enhanced "blood-pool" activity of ^{99m}Tc MDP is common to both acute osteomyelitis and cellulitis. The distinction between osseous and soft-tissue infection is made on the delayed images where focally increased activity in bone favors osteomyelitis, whereas normal activity distribution or low-grade diffuse uptake in the underlying bone signifies adjacent cellulitis.

Recent traumatic fracture, osteomyelitis, Paget's disease, and osteoid osteoma show increased activity in all three phases and, thus, cannot be differentiated readily by three-phase scintigraphy.

Periarticular cellulitis and septic arthritis both exhibit hyperperfusion and hyperemia about the joint and cannot be distinguished by these criteria alone.

As indicated by the above, three-phase bone scintigraphy is of primary use in distinguishing an osseous lesion from a soft-tissue abnormality, but is of relatively little value in differentiating between various types of active osseous lesions.

References

1. Maurer AH, Chen DCP, Camargo EE, Wong DF, Wagner HN Jr. Utility of three-phase skeletal scintigraphy in suspected osteomyelitis [Concise Communication]. *J Nucl Med* 1981;22:941-949.
2. Shafer RB, Edeburn GF. Can the three-phase bone scan differentiate osteomyelitis from metabolic or metastatic bone disease? *Clin Nucl Med* 1984;9:373-377.

Items 14-18: Scintigraphy in Osteomyelitis

Answers: 14, T; 15, T; 16, F; 17, T; 18, F

The reduction of ^{67}Ga uptake to levels still above normal after treatment of acute osteomyelitis is seen frequently and is not a harbinger of chronic osteomyelitis. It probably represents the sterile component of bone repair. The corresponding ^{99m}Tc MDP images often continue to show intense activity after the infection passes from the septic phase to the bone repair phase. In chronic osteomyelitis, on the other hand, low-grade ^{67}Ga concentration often is seen in the same distribution as ^{99m}Tc MDP. In this setting, infection is more reliably diagnosed when the ^{67}Ga uptake is much greater than that of ^{99m}Tc MDP, or when intense focal ^{67}Ga uptake is seen within the larger region of remodeling depicted by bone scintigraphy.

Although literature reports exist to the contrary, the consensus is that ^{111}In leukocyte scintigraphy generally is less sensitive for detecting chronic than acute osteomyelitis, presumably reflecting the greater fraction of mononuclear cells rather than polymorphonuclear leukocytes, in the inflammatory response with chronic infection.

Both osteosarcomas and acute osteomyelitis avidly concentrate ^{67}Ga and ^{99m}Tc MDP, so that they cannot be distinguished on that basis alone. However, osteosarcoma more likely will show extension of the accumulation of the two radiopharmaceuticals into the adjacent soft tissues.

References

1. Mido K, Navarro DA, Segall GM, McDougall IR. The role of bone scanning, gallium and indium imaging in infection. In: Fogelmann I, ed. *Bone Scanning in Clinical Practice*. London: Springer-Verlag, 1987: 105-120.

For further in-depth information, refer to the syllabus pages in Nuclear Medicine Self-Study I.